Article

TRANSPARENT PROCESS

EMBO reports

Long noncoding RNA EGOT negatively affects the antiviral response and favors HCV replication

Elena Carnero[1,†], Marina Barriocanal[1,†], Celia Prior[1], Juan Pablo Unfried[1], Victor Segura[2], Elizabeth Guruceaga[2], Mónica Enguita[1], Cristian Smerdou[1], Pablo Gastaminza[3] & Puri Fortes[1,*]

Abstract

The role of long noncoding RNAs (lncRNAs) in viral infection is poorly studied. We have identified hepatitis C virus (HCV)-Stimulated lncRNAs (CSRs) by transcriptome analysis. Interestingly, two of these CSRs (PVT1 and UCA1) play relevant roles in tumorigenesis, providing a novel link between HCV infection and development of liver tumors. Expression of some CSRs seems induced directly by HCV, while others are upregulated by the antiviral response against the virus. In fact, activation of pathogen sensors induces the expression of CSR32/EGOT. RIG-I and the RNA-activated kinase PKR sense HCV RNA, activate NF-κB and upregulate EGOT. EGOT is increased in the liver of patients infected with HCV and after infection with influenza or Semliki Forest virus (SFV). Genome-wide guilt-by-association studies predict that EGOT may function as a negative regulator of the antiviral pathway. Accordingly, EGOT depletion increases the expression of several interferon-stimulated genes and leads to decreased replication of HCV and SFV. Our results suggest that EGOT is a lncRNA induced after infection that increases viral replication by antagonizing the antiviral response.

Keywords EGOT; HCV; lncRNAs; PKR; SFV
Subject Categories Immunology; Microbiology, Virology & Host Pathogen Interaction; RNA Biology
DOI 10.15252/embr.201541763 | Received 16 November 2015 | Revised 3 May 2016 | Accepted 12 May 2016 | Published online 9 June 2016
EMBO Reports (2016) 17: 1013–1028

Introduction

The competition between viruses and the immune system is one of the drivers of evolution. During infection, viral factors are sensed by canonical (i.e., RIG-I (retinoic acid-inducible gene 1) or TLRs (Toll-like receptors)) and non-canonical (i.e., PKR) cellular receptors, which trigger activation of NF-κB and interferon regulatory transcription factors (IRFs) leading to expression of type I interferons (IFN) and proinflammatory cytokines [1]. This initiates the cellular antiviral response. Viruses have evolved to express factors that block the antiviral pathways [1]. In turn, the IFN response has evolved to hinder viral infection by affecting the steps required for viral viability. IFN binding to its receptor activates the JAK/STAT pathway and the expression of IFN-stimulated genes (ISGs). Most ISGs are antiviral genes that function to increase cell sensitivity against infections or to block viral entry, replication, translation, stability, or release [1]. Interestingly, some ISGs function as negative regulators of the IFN pathway that limit the duration and strength of the response and are essential in helping the cell to return to homeostasis [1]. Importantly, some of these IFN-induced negative regulators of the IFN pathway have proviral functions [2].

Most ISGs and the cellular factors described as proviral or antiviral are proteins. However, it has been recently shown that the IFN pathway also regulates the expression of several long noncoding RNAs (lncRNAs) [3–6]. This is not surprising, as lncRNAs are thought to be at least as numerous as protein-coding genes and the few lncRNAs studied to date have been shown to play relevant roles in cell proliferation, differentiation, and homeostasis [7]. LncRNAs are transcripts longer than 200 nucleotides with no identifiable protein-coding potential. LncRNA genes are similar to mRNA genes at the chromatin and sequence levels, and they share common mechanisms for transcription and processing. However, lncRNAs are more cell type specific, less abundant, and less conserved than mRNAs. Interestingly, lncRNAs may regulate the expression of distal or neighboring genes by different mechanisms [7].

In line with this, it has been recently shown that many IFN-regulated lncRNA genes function to tune the expression of ISGs located nearby by acting as positive or negative regulators [3–6]. Some of the IFN-induced lncRNAs are also upregulated after viral infection [4,5]. Infection with HIV or influenza virus (Flu), among others, has been shown to alter the expression of cellular lncRNAs [8–10]. Thus, HIV infection increases the expression of NEAT1 and Flu infection increases lncRNA VIN and decreases NRAV. Interestingly, downregulation of NEAT1 increases HIV replication, while downregulation of VIN or NRAV decreases efficiency of Flu

1 Department of Gene Therapy and Hepatology, Center for Applied Medical Research (CIMA) and IdiSNA, Navarra Institute for Health Research, University of Navarra, Pamplona, Spain
2 Bioinformatics Unit, CIMA and IdisNA, University of Navarra, Pamplona, Spain
3 National Center of Biotechnology CNB/CSIC, Madrid, Spain
*Corresponding author. Tel: +34 948194700; Fax: +34 948194717; E-mail: pfortes@unav.es
†These authors contributed equally to this work

infection. In fact, NRAV is a negative regulator of ISG transcription. This demonstrates that viral infection can alter the expression of cellular lncRNAs with antiviral or proviral functions. However, in general, few virus-regulated lncRNAs have been identified and their function has been poorly studied [11].

In this study, we asked whether the expression of cellular lncRNAs is altered after infection with hepatitis C virus (HCV). HCV is a hepatotropic virus whose infection affects more than 170 million people worldwide and frequently leads to liver cirrhosis and hepatocellular carcinoma [12]. In this study, we examined the transcriptome of control liver cells and cells infected with HCV. Then, we identified lncRNAs whose expression is deregulated in infected cells. The best upregulated candidates have been validated and termed CSRs, after HCV-Stimulated RNAs. Interestingly, several CSRs have been described as oncogenes, providing a link between HCV infection and the development of liver tumors. We show that some of the CSRs are upregulated by treatment with pIC or IFN, indicating that they respond to the antiviral response induced against infection. In fact, stimulation of RIG-I or PKR by HCV activates the expression of CSR32/EGOT. Inhibition of EGOT leads to increased levels of several ISGs and to decreased viral replication. Therefore, EGOT is a proviral lncRNA induced after infection that regulates the antiviral response.

Results

Identification of lncRNAs regulated by HCV

To identify lncRNAs that respond to HCV, we infected HuH7 cells with a moi of 0.3 of the JFH-1 strain of HCV for 6 days. At this time, most of the cells were infected with the virus as evaluated by immunofluorescence against HCV core protein. RNA isolated in three independent experiments from these HCV-infected cells and from control HuH7 cells was used to hybridize an Agilent array that evaluates expression of 27,958 Entrez genes and 7,419 lncRNAs. Analysis of the array showed that many of the coding genes whose expression is altered with a high statistical significance ($B > 0$) have already been described as changing levels after HCV infection (Fig 1A and B) [13–15]. These include genes related to immunity and defense (IL8, MX1, IRF1, or members of the CXCL family), genes involved in oxidative stress and detoxification (SOD2 or CYP1A1), and genes involved in cell proliferation, cholesterol synthesis, or fatty acid metabolism. Similar functions were also found by Ingenuity analysis of the data (Appendix Fig S1). We selected the probes that showed a significantly altered expression by HCV infection and that were described in the array as lncRNAs (505 probes with $B > 2$) (Fig 1C). We excluded from further analysis miss-annotated probes that corresponded to coding genes or seemed to be 3′UTR extensions of coding genes. Seventy-three putative lncRNA genes were identified as upregulated and 82 as downregulated with a log fold change higher than 2 (FC > 2) (Appendix Table S1).

We decided to focus on all those transcripts identified in the array that were significantly upregulated by HCV infection ($B > 2$ and FC > 2) and that had been previously annotated in public databases (GENCODE, ENSEMBL, RefSeq, GenBank, and Rfam). We called them CSR, from HCV-Stimulated RNAs. We also decided to

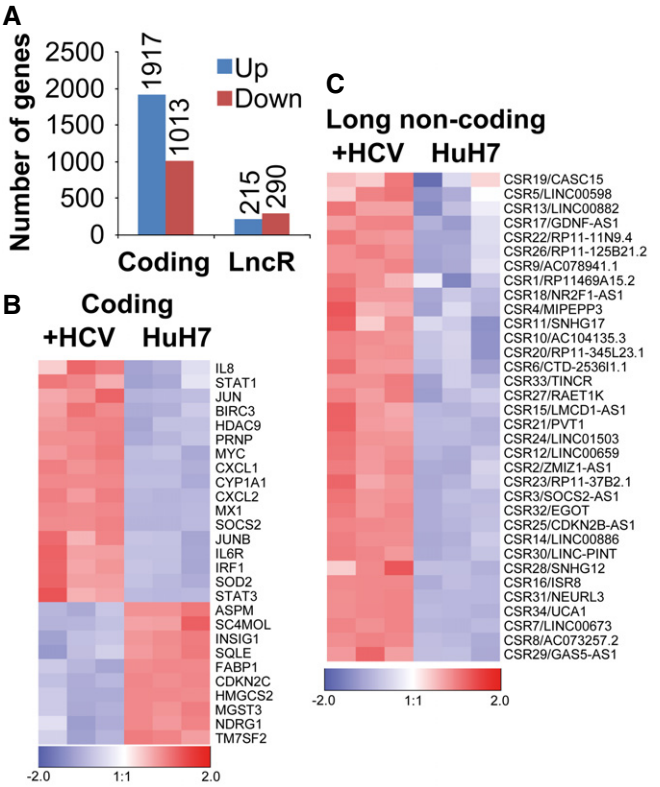

Figure 1. Transcriptome analysis of HCV-altered genes.

A–C RNA was isolated from control HuH7 cells or cells infected with HCV for 6 days in three independent experiments. These RNAs were hybridized to a SurePrint Agilent array, and the number of coding or lncRNA (LncR) genes whose expression is up- or downregulated (B > 2) is shown (A). A heatmap of coding (B) and lncRNA (C) genes relevant for this study is also shown.

study CSR30 and CSR33, which had a fold change lower than 2 but corresponded to interesting lncRNAs such as LINC-PINT and TINCR [16,17]. Out of the 35 CSRs, 26 also showed increased levels in RNASeq data of HCV-infected cells compared to controls (Appendix Fig S1; Appendix Table S2). None of the 35 CSRs selected was liver specific according to their analysis using transcriptomes from the Human BodyMap (Appendix Fig S2; https://www.ebi.ac.uk/gxa/experiments/E-MTAB-513).

HCV infection increases the expression of several lncRNAs

To validate the effect of HCV infection on the expression of these 35 CSRs, their levels were evaluated by qRT–PCR in HuH7 cells uninfected or infected with a moi 0.3 of HCV for 6 days. The fold change observed for each candidate in HCV-infected versus non-infected cells is shown in Fig 2A. The expression of most candidates is induced after HCV infection, with the exception of CSR9 and CSR16, which we failed to detect above background levels. Fourteen candidates showed apparent low expression levels by qRT–PCR and were discarded. CSR28 was also discarded as it transcribes SNHG12, a host of small nucleolar RNAs. We opted to focus on the remaining CSRs that displayed the highest upregulation after HCV infection (FC > 7): CSR3, 6, 7, 19, 20, 21, 26, 31, 32, and 34

(Appendix Table S3). Interestingly, some of these lncRNAs are induced several hundred-fold upon infection. To study in more detail the response of these candidates to HCV, we evaluated their expression by qRT–PCR in controls or in cells infected for 12, 24, 48, or 72 h with a moi of 0.3 of HCV JFH-1. The results show that the CSRs increase their expression as infection progresses (Fig 2B).

Analysis of subcellular localization and coding potential of CSRs

Extensive bioinformatic analyses using ORF Finder (NCBI), PhyloCSF, CPAT, and databases such as LNCipedia predict that the selected CSRs are noncoding RNAs (Fig EV1A and B; see Materials and Methods for details [18–23]). Overall, these analyses indicate that (i) all putative ORFs that could be translated are shorter than 100 aa, (ii) bioinformatic analyses predict a low coding probability, and (iii) sequences of the evaluated CSRs are absent from databases related to translation. The only exception is NEURL3/CSR31. Some NEURL3 transcripts could be translated to ORFs longer than 100 aa, have a coding probability above the noncoding threshold, and NEURL3 homologue in rat may encode for an E3 ubiquitin protein ligase. However, NEURL3 is a noncoding pseudogene according to ENCODE. Pseudogenes have a higher possibility of giving false-positive results in programs such as PhyloCSF. The reason for this is that pseudogenes are similar to their parental coding genes, and PhyloCSF evaluates conservation to predict coding capacity. Therefore, further experiments should be performed to determine whether NEURL3 is indeed a coding gene.

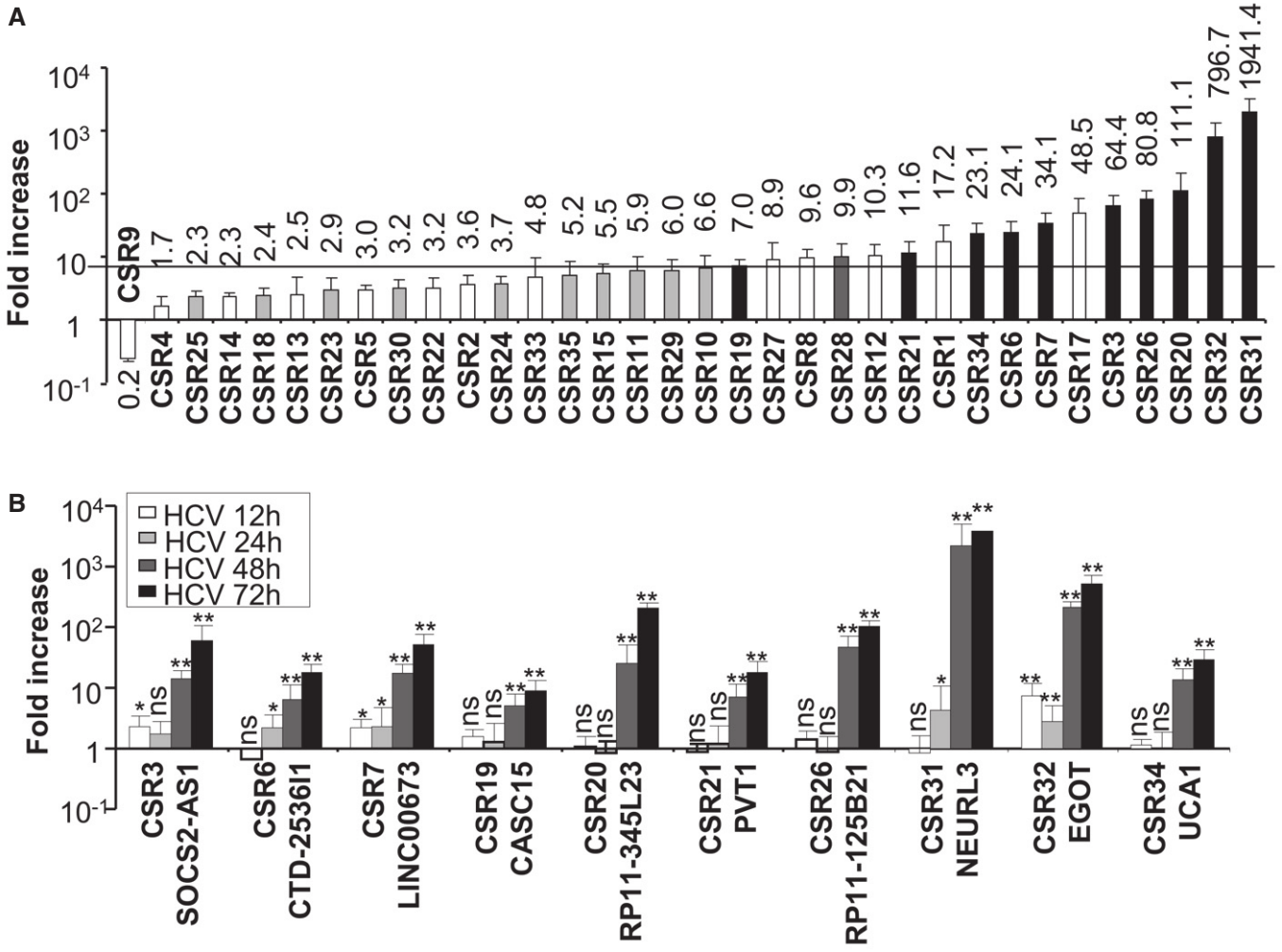

Figure 2. Long noncoding RNAs are induced after HCV infection.

A Expression of CSR1 to CSR35 was evaluated by qRT–PCR in RNA isolated from control cells or cells infected with a moi 0.3 of HCV for 6 days. GAPDH levels were also measured and used as a reference. Fold increase of each CSR in infected versus control cells is indicated at the top of each bar. A line has been drawn to mark the position of sevenfold, our arbitrary cutoff value. Black bars, candidates expressed to good levels that increase more than sevenfold; white bars, candidates expressed poorly according to the parameters described in Appendix Table S2; gray bars, candidates expressed to good levels induced less than sevenfold. CSR28 bar was shaded to highlight that this candidate was not evaluated further.

B HuH7 cells were infected with a moi 0.3 of HCV for 0, 12, 24, 48, and 72 h and analyzed as in (A).

Data information: The experiments were performed in triplicate at least twice, and each value shows the average of the results ($n = 6$). Error bars indicate standard deviations and asterisks mark significant differences obtained with a two-tailed nonparametric Mann–Whitney *U*-test (ns, nonsignificant, $*P \leq 0.05$, $**P \leq 0.01$).

The subcellular localization of CSRs was evaluated by qRT–PCR in nuclear or cytoplasmic fractions of HCV-infected cells. As expected, the nuclear lncRNA MALAT1 was preferentially nuclear while the coding GAPDH mRNA was enriched in the cytoplasm (Fig EV1C). Similarly, CSR3, 6, 7, 20, 31, and 34 accumulate preferentially in the cytoplasm while CSR19, 21, 26, and 32 accumulate preferentially in the nucleus. In fact, the nuclear localization of lncRNAs CSR21/PVT1 and the cytoplasmic localization of CSR34/UCA1 have already been reported [24,25]. The preferential nuclear localization of CSR19, 21, 26, and 32, away from the site of translation, together with the bioinformatic analyses, suggests that these CSRs are noncoding RNAs.

Some CSRs respond to the antiviral pathway while others seem to be induced directly by HCV infection

Once we established that most of the selected CSRs are transcripts with poor coding potential induced after infection with HCV, we sought to understand the mechanism of upregulation. CSRs may be upregulated directly by HCV infection or by the antiviral response induced by infection. To determine whether the IFN pathway could affect CSR expression, we treated HuH7 cells with high doses (10,000 U/ml) of IFNα2 for 3 days and compared the expression of the CSRs in IFN-treated versus untreated or HCV-infected cells. Under these conditions, it is still possible to detect increased expression of genes that are induced early after IFN treatment but also increased levels of genes that respond to a secondary wave of the IFN response [4]. The results show that IFN treatment significantly increases the expression of CSR31 and 32 (Fig 3A). Unlike CSR32, CSR31 was also induced with lower doses of IFN and with only 6 h of IFN treatment (Appendix Fig S3A and B). However, the levels of CSR31 and CSR32 are more than a hundred-fold lower in IFN-treated cells than in cells infected with HCV for 6 days at moi 0.3 (Fig 3A). A synergism between IFN and HCV infection was not observed as cells treated with the combination of HCV (moi 0.3 for 6 days) and IFN (10,000 U/ml during the last 3 days of infection) have CSR levels similar to those of cells that have only been infected with HCV at moi 0.3 for 6 days. Note that under these conditions, there is only a minor effect of IFN on viral replication (Appendix Fig S3C).

CSR expression could be induced in response to the activation of antiviral sensors. These sensors detect dsRNA regions of viral genomes or viral replication and induce the expression of IFN and other antiviral genes [26]. In fact, CXCL10 mRNA, used as a positive control, and several CSRs were significantly induced after transfection of HuH7 cells with the dsRNA analogue poly I:C (pIC) for 8 h, albeit at lower levels than by HCV infection (Fig 3B). However, CSR19, 21, 26, and 34 were neither induced by IFN or pIC nor by infection with other viruses tested, such as influenza or Semliki Forest virus (SFV), suggesting that they could be lncRNAs that are induced specifically by HCV infection (Appendix Fig S3D).

CSR32/EGOT is also induced after infection with other RNA viruses and by TLR induction

Considering all the results obtained, we decided to study CSR32, the eosinophil granule ontogeny transcript (EGOT) in more detail. EGOT was chosen because it is highly induced after infection with

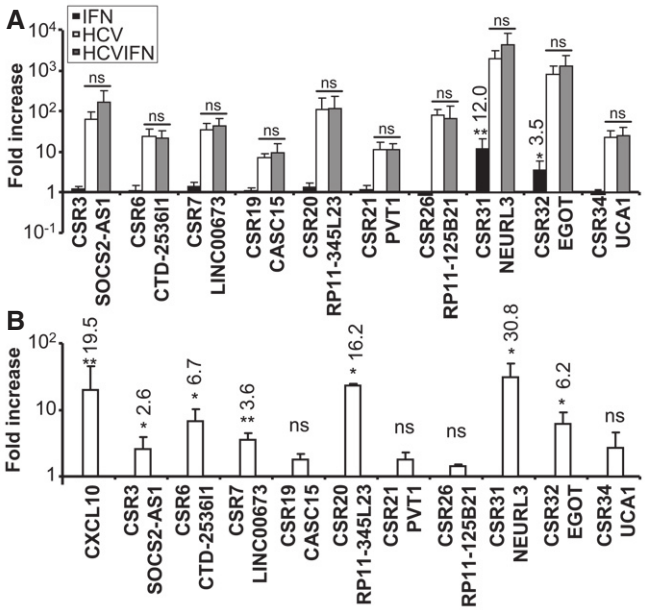

Figure 3. Some CSRs are induced by IFN or by the dsRNA response pathway.

A HuH7 cells were mock-treated, treated with 10,000 U/ml of IFNα for three days, infected with HCV for six days or infected with HCV for six days, and treated with IFN during the last three days of infection. The levels of the indicated CSRs were quantified by qRT–PCR. GAPDH mRNA was also measured and used as a reference. Fold increase of each CSR in treated/infected versus control cells is shown.

B Control cells or cells collected 8 h post-transfection with pIC. The levels of CXCL10 mRNA and the indicated CSRs were quantified by qRT–PCR. GAPDH mRNA was also measured and used as a reference. Fold increase of each CSR in treated versus control cells is shown. Fold changes higher than 2 are indicated at the top of each bar.

Data information: The experiments were performed at least twice in triplicate, and each value shows the average ($n = 6$). Error bars indicate standard deviations and asterisks mark significant differences (ns, nonsignificant; $*P \leq 0.05$, $**P \leq 0.01$) obtained with a two-tailed nonparametric Mann–Whitney *U*-test.

HCV, has poor coding potential, and accumulates preferentially in the nucleus after infection with HCV. In fact, the EGOT region of the genome has a relatively high level of histone 3 lysine 4 monomethylation over trimethylation, indicating that EGOT could be an enhancer RNA [27] (Fig EV2A). Finally, synteny alignments between different species and evaluation of the ESTs expressed in those regions suggest that EGOT has homologues in primates and rodents, which could indicate a conserved function through evolution [28].

We first determined that EGOT is a polyadenylated transcript, as increased levels of EGOT were observed in HCV-infected cells compared to non-infected controls when the RT–PCR was performed with oligodT instead of random primers (Fig EV2B). RACE experiments confirmed that the sequence of EGOT expressed in HuH7 cells is properly annotated in the ENCODE and RefSeq databases except at the 5′ end, where it extends 32 additional nucleotides (Fig EV2C). EGOT cDNA was cloned and sequenced to confirm the splice junction. EGOT cDNA was transcribed *in vitro* and quantified. RT–PCR with serial dilutions of this RNA was performed and allowed us to

calculate the absolute numbers of cellular EGOT, indicating that there are ~8–15 molecules of this lncRNA per cell in cells infected with HCV for 48 h. Similar experiments performed with UCA indicated that there are ~60–90 molecules of UCA1 per HuH7 cell infected with HCV for 48 h.

Then, as EGOT is induced after treatment with pIC, we speculated that it might also be induced after infection with other RNA viruses. Therefore, we evaluated EGOT levels in HuH7 cells infected for 4, 8, or 24 h with influenza virus or with SFV at a moi of 10, which caused cytopathic effects at 24 h post-infection (hpi). Infection with influenza, an RNA virus that replicates in the nucleus, and SFV, an RNA virus that replicates in the cytoplasm, induces expression of EGOT at early times post-infection (Fig 4A and B). Surprisingly, EGOT levels increased dramatically at later times post-SFV infection. As both SFV and HCV replicate in the cytoplasm and strongly induce EGOT expression, we hypothesized that cytoplasmic viral replication could be required for EGOT induction. In order to test this, we infected HuH7 cells with a moi 0.3 of HCV for 72 or 96 h. Viral replication was inhibited by treatment with a cocktail of inhibitors (sofosbuvir, daclatasvir, and ribavirin) for the last 24 or 48 h of infection, respectively. The cocktail of inhibitors did not affect EGOT levels in the absence of infection (data not shown). Inhibition of replication was confirmed by evaluation of viral RNA levels (Fig 4C, left graph). EGOT levels also decreased drastically when viral replication was inhibited (Fig 4C, right graph). Therefore, EGOT could increase in response to viral genomes or in response to any of the multiple effects caused by replication. To determine whether HCV genomes can induce EGOT, EGOT levels were evaluated in control cells, cells infected with a moi of 0.3 of HCV for 5 h (immediately after infection), cells infected with UV-treated HCV for 12 h, or cells infected with HCV for 48 h in the presence of a cocktail of inhibitors of replication. In all cases, although low levels of viral RNA were detected, EGOT expression was significantly increased compared to mock-infected cells (Fig 4D and data not shown). Finally, we evaluated whether EGOT could also increase in response to other pathogen-associated molecular patterns (PAMPs). As HuH7 cells express TLR4 (LPS sensor) and TLR7 (sensor for ssRNA and agonists like Imiquimod), cells were treated with LPS or Imiquimod for 24 h. The treatment induced CXCL10 mRNA, used as a positive control, and increased significantly the levels of EGOT (Fig 4E). Treatment of the cells with cytokines such as oncostatin or IL-6 resulted in increased levels of IL-15 receptor mRNA, used as a control, but did not alter the expression of EGOT (Fig 4E and data not shown).

EGOT is induced by RIG-I and PKR activation in HCV-infected cells

Collectively, our results indicate that EGOT is increased in response to different PAMPs, including pIC or the viral RNA genome. As TLR3 (pIC sensor) is poorly expressed in HuH7 cells, the cytoplasmic RIG-I could be the major sensor of pIC and viral RNA. To test whether RIG-I may mediate EGOT induction, cells transfected with siRNAs that target RIG-I (siRIG-I) were infected with HCV for 48 h. At this time, the levels of RIG-I mRNA, CXCL10 mRNA, a

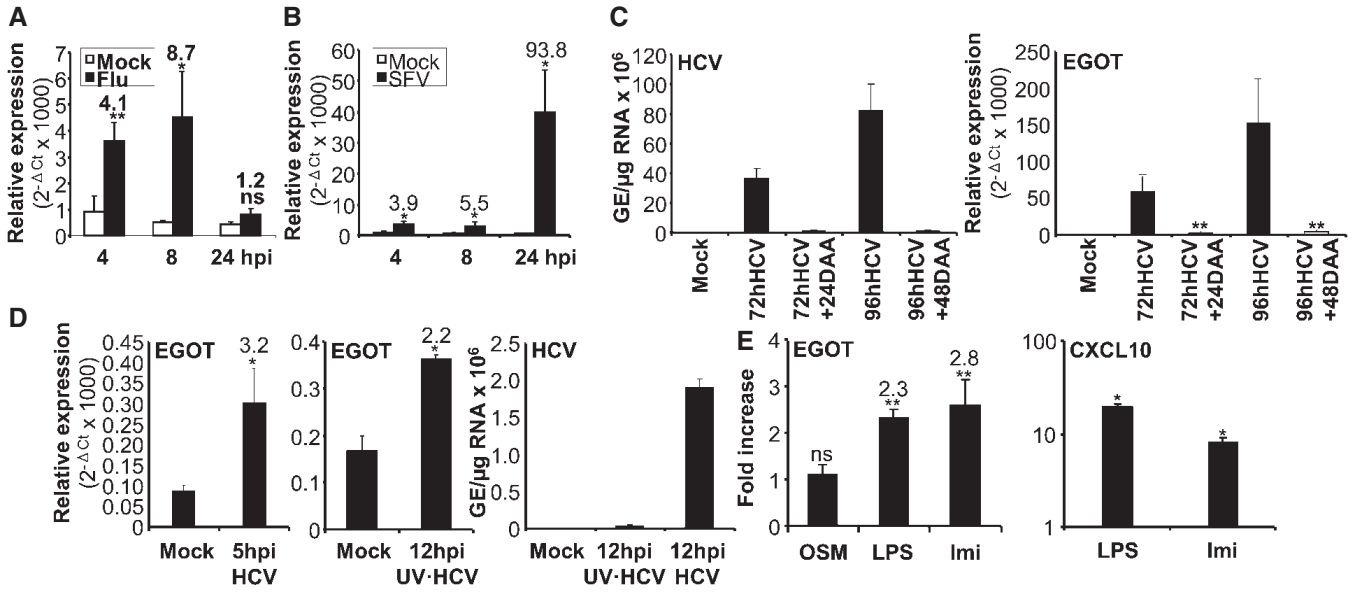

Figure 4. EGOT increases after infection with influenza, SFV or HCV and by TLR activation.

A–D Cells were infected with a moi 10 of influenza (Flu) (A) or SFV (B) for 4, 8, and 24 h, or with HCV for 5, 12 (D), 72, and 96 h (C). Some infected cells were treated with inhibitors of replication (DAA) the last 24 or 48 h of infection (C). All HCV infections were done with a moi of 0.3 except the one examined at 12 hpi, which was performed with a moi of 1 of control HCV virus or UV-irradiated virus (UV-HCV). Levels of EGOT or genome equivalents (GE) of HCV RNA per µg of total RNA were calculated by qRT–PCR in RNA isolated from the control or infected HuH7 cells. GAPDH expression was used as a reference to calculate the relative levels of each transcript.

E Cells were treated with oncostatin M (OSM), LPS, or Imiquimod (Imi) for 24 h. Levels of EGOT and CXCL10 mRNA were calculated by qRT–PCR in RNA isolated from the control or treated HuH7 cells. GAPDH expression was used as a reference to calculate the relative levels of each transcript.

Data information: The experiments were performed twice in triplicate ($n = 6$). Each value shows the average and error bars indicate standard deviations. Asterisks mark significant differences (ns, nonsignificant; *$P \leq 0.05$, **$P \leq 0.01$) obtained with a two-tailed nonparametric Mann–Whitney *U*-test.

Figure 5. EGOT is induced by RIG-I and PKR through NF-κB.

A HuH7 cells were transfected with control siRNAs (siCtrl) or siRNAs that target RIG-I (siRIG-I); 48 h later, cells were infected with a moi 0.3 of HCV and evaluated at 48 hpi. The relative levels of EGOT and RIG-I were evaluated by qRT–PCR in RNAs isolated from these samples. GAPDH expression was used as a reference to calculate the relative levels of each transcript. Fold increase of treated versus control cells was also calculated. Percentage versus 100% of control samples is shown.

B HuH7.5 cells were mock-infected or infected with moi 0.3 of HCV for 72 h. The relative levels of EGOT mRNA were evaluated by qRT–PCR in RNAs isolated from these samples. The relative levels of EGOT and genome equivalents of HCV (GE)/μg of total RNA were also quantified by qRT–PCR. GAPDH expression was used as a reference.

C HuH7 cells were transfected with control siRNAs (siCtrl) or siRNAs that target PKR (siPKR), and 48 h later, cells were infected with a moi 0.3 of HCV and evaluated at 48 hpi. The relative levels of EGOT and PKR mRNA were evaluated by qRT–PCR in RNAs isolated from these samples. GAPDH expression was used as a reference to calculate the relative levels of each transcript. Fold increase of treated versus control cells was also calculated. Percentage versus 100% of control samples is shown.

D HuH7 cells were transfected with increasing amounts (0.03, 0.06, 0.125, 0.25, or 0.5 μg per M6 plate) of a plasmid expressing PKR (pPKR) and collected 48 h post-transfection. The relative levels of EGOT mRNA were evaluated by qRT–PCR in RNAs isolated from these samples. GAPDH expression was used as a reference. Fold increase of treated versus control cells was also calculated.

E HuH7 cells were mock-transfected (–) or transfected with 0.5 μg per M6 dish of pPKR (+), and 48 h later, cells were transfected with or without 10 μg of pIC or infected with a moi 0.3 of HCV. Cells were collected 8 h post-transfection with pIC or 48 hpi with HCV. The relative levels of EGOT mRNA were evaluated by qRT–PCR in RNAs isolated from these samples. GAPDH expression was used as a reference.

F Schematic representation of RIG-I and PKR pathways. Indicated is PKR inhibition of translation and induction of NF-κB and IRF3 by RIG-I and PKR. NF-κB response to TNFα and activation of EGOT is also indicated.

G, H HuH7 cells were mock-transfected or transfected with plasmids expressing a dominant negative form of IRF3 (G; DNIRF3), or a superrepressor of NF-κB (H; pIKB (SA)). One day after transfection, cells were infected with HCV and collected at 48 hpi. The relative levels of EGOT and CXCL10 mRNA were evaluated by qRT–PCR in RNAs isolated from these samples. GAPDH expression was used as a reference to calculate the relative levels of each transcript. Fold increase of treated versus control cells was also calculated.

I Cells were treated with 20 ng/ml of TNFα for 6 or 12 h. The relative levels of EGOT mRNA were evaluated by qRT–PCR in RNAs isolated from these samples. GAPDH expression was used as a reference. Fold increase of treated versus control cells was also calculated.

Data information: The experiments were performed at least twice in triplicate ($n = 6$). Average values are shown and error bars indicate standard deviations. Asterisks mark significant differences (ns, nonsignificant; *$P \leq 0.05$, **$P \leq 0.01$, and ****$P \leq 0.0001$) obtained with a two-tailed nonparametric Mann–Whitney *U*-test.

downstream target of RIG-I activation, and EGOT were reduced in cells expressing siRIG-I compared to control cells (Figs 5A and EV3A). To determine whether RIG-I is essential for EGOT induction, we used HuH7.5 cells, which harbor inactive RIG-I. HuH7.5 cells infected with HCV for 72 h also showed increased levels of EGOT compared to uninfected cells (Fig 5B). This indicates that another RNA sensor could be inducing EGOT. It has been reported that PKR can be activated by pIC and the HCV viral genome to induce the expression of several genes [29]. We also found more PKR phosphorylation in cells treated with pIC for 8 h or in cells infected with HCV for 48 h than in control cells, as evaluated by Western blot (Fig EV3B). Therefore, we asked whether PKR could induce EGOT expression. PKR expression was inhibited by siRNAs (siPKR) in HuH7 cells and 2 days later, cells were infected for 48 h with HCV. At this time point, cells expressing siPKR showed decreased PKR mRNA, decreased levels of the PKR target gene ISG15, decreased HCV replication, as has been already shown [30], and decreased levels of EGOT (Figs 5C and EV3C and D). In agreement with a role of PKR in EGOT expression, transfection of HuH7 cells with increasing concentrations of a plasmid expressing PKR resulted in increased PKR and PKR phosphorylation and in the upregulation of EGOT (Figs 5D and EV3B and E). In summary, EGOT is induced in response to pIC or HCV infection and this response is enhanced by overexpression of PKR (Fig 5E).

PKR and RIG-I induce transcription by activation of IRF3 and NF-κB (Fig 5F; [29]). To evaluate which transcription factor mediates EGOT activation, we used a dominant negative of IRF3 (DNIRF3), which lacks the DNA binding domain [31] and the NF-κB superrepressor IKB(SA), a mutated IKB at phosphorylation sites S32 and S36 that binds NF-κB but cannot be phosphorylated and degraded, and therefore hinders NF-κB activation [32]. To evaluate the functionality of DNIRF3, cells were transfected with a firefly luciferase reporter that responds to IRF3 ((PRDIII-I)4-Luc; [33]), a plasmid expressing IRF3 and a control plasmid or the plasmid expressing DNIRF3. IKB(SA) repressor was tested in cells transfected with a luciferase reporter induced by NF-κB (NF-κB 3xLuc; [34]) and a control plasmid or the plasmid expressing IKB(SA). Then, the cells were treated with LPS for 24 h to induce NF-κB activity. A plasmid expressing Renilla luciferase was also transfected in all cases for normalization. Forty-eight hours after transfection, Renilla and firefly luciferases were quantified. As expected, normalized firefly luciferase levels were decreased in those cells expressing the inhibitors as compared to control cells (Fig EV3F and G). After this validation, plasmids expressing the inhibitors were transfected into cells, then cells were infected with HCV for 48 h, and EGOT levels were measured by qRT–PCR. Expression of the dominant negative of IRF3 decreased expression of CXCL10, used as a positive control, but did not affect EGOT levels (Fig 5G). In turn, expression of IKB (SA) decreased CXCL10 mRNA and also EGOT (Fig 5H). In agreement, EGOT also increased strongly in cells treated with TNFα, an inducer of NF-κB, for 6 or 12 h (Fig 5I). In fact, the promoter of EGOT contains binding sites for NF-κB, as identified by ChIP-Seq analysis performed by ENCODE and evaluation of conserved transcription factor binding sites deposited at UCSC (Appendix Table S3; Fig EV2).

CSR32/EGOT is also induced in the liver of HCV-infected patients

We used two independent cohorts of patients to determine that EGOT was also significantly increased in the liver of HCV-infected patients as compared to controls (Fig 6A). We did not observe differences in the levels of other CSRs, such as CSR14 or 23, between controls and HCV-infected livers (data not shown). These CSRs were taken as controls as they show good expression levels in the liver, but they are not markedly increased after HCV infection in HuH7 cells (Fig 2A, Appendix Fig S2). HCV RNA and TNFα mRNA were

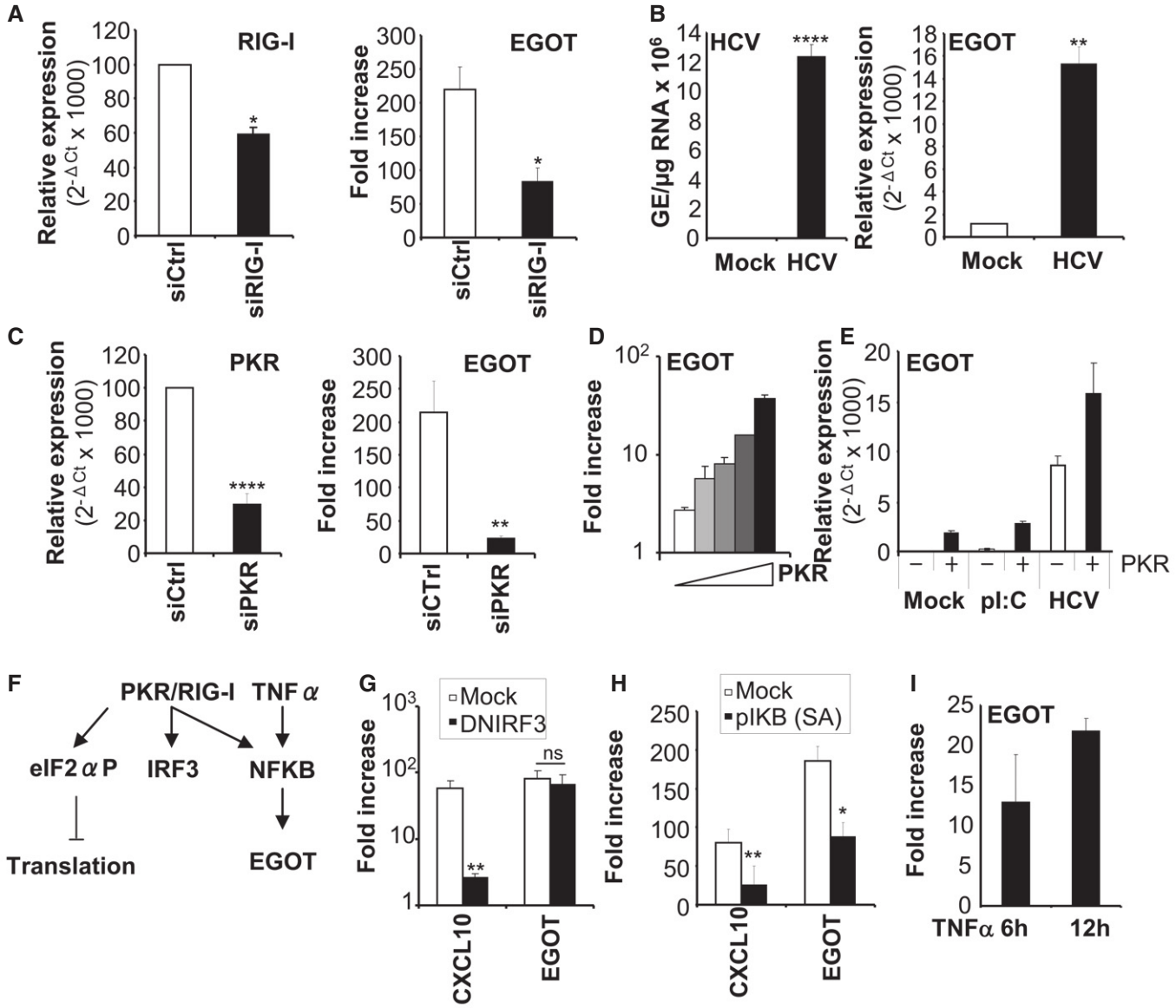

Figure 5.

also evaluated in the livers of the second cohort of patients. We observed a significant correlation between TNFα mRNA and EGOT but not between HCV RNA and EGOT (Fig 6B). This suggests that TNFα could be a major driver of EGOT expression in the liver.

Given that several CSRs have been described as oncogenes, we paid special attention to EGOT expression in patients with hepatocellular carcinoma (HCC). We observed no altered expression of EGOT in these patients as compared to HCV-infected patients without HCC (Fig 6A and data not shown). Similar results were obtained in mice. We quantified the levels of the putative mouse homologue of EGOT (mEGOT) identified by synteny [28]. We observed no differences in the expression levels of mEGOT comparing healthy mouse livers ($n = 7$), and peritumor ($n = 17$) or tumor tissue ($n = 23$) obtained from HCCs induced in mice 9 months after treatment with diethylnitrosamine (data not shown). In turn, the mouse homologue of PVT1 was significantly increased in tumor samples compared to healthy livers (data not shown).

EGOT allows efficient viral replication

To evaluate the role of EGOT in viral infection, we depleted EGOT from HCV-infected HuH7 cells with two independent gapmers targeting EGOT. Cells were transfected with the gapmers 1 day prior to infection with a moi 0.3 of HCV and collected at 48 hpi. The specific gapmers decreased the levels of EGOT efficiently and did not affect cell viability (Fig 7A; Appendix Fig S4). Under these conditions, viral genomes, viral titer, and viral core and NS3 proteins were significantly decreased (Fig 7B–D). Therefore, EGOT is required for efficient HCV replication.

Given that EGOT is also upregulated after infection with SFV, we evaluated the role of EGOT in SFV infection. As was done for HCV, HuH7 cells were first transfected with the gapmers targeting EGOT and controls, and then, cells were infected with a moi of 0.01 of SFV and collected at 24 hpi. The cells with decreased levels of EGOT produced fewer viral genomes and fewer SFV virions (Fig 7E–G).

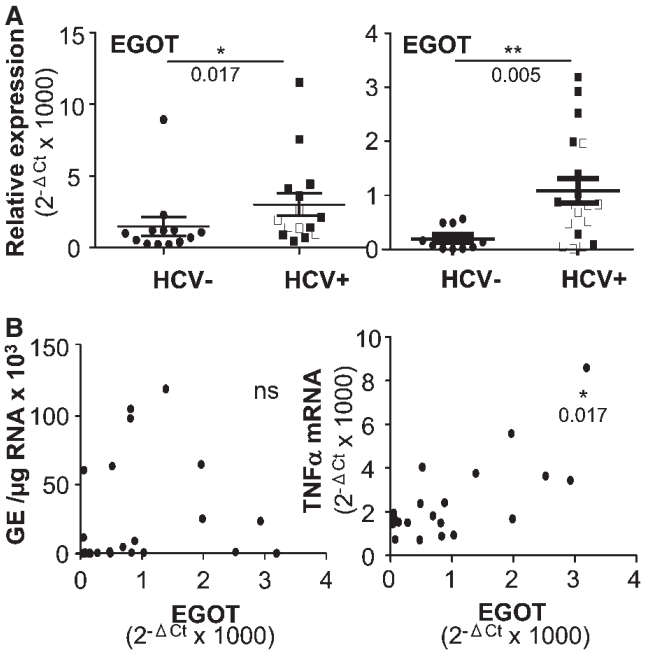

Figure 6. EGOT levels are increased in the liver of patients infected with HCV.

A, B Expression levels of EGOT (A) and genome equivalents of HCV (GE)/µg of total RNA and TNFα mRNA (B) were evaluated in two cohorts of HCV-negative (n = 13/n = 10) and HCV-positive (n = 15/n = 19) patients by qRT–PCR. Measurements obtained with patients with HCC are indicated with white squares. Statistical significance was calculated using a two-tailed nonparametric Mann–Whitney U-test. Correlation between EGOT and HCV RNA or TNFα mRNA was calculated with Spearman's correlation coefficient. Asterisks mark significant differences (ns, nonsignificant; *$P \leq 0.05$, **$P \leq 0.01$).

This indicates that EGOT expression may be required for the efficient replication of several viruses.

EGOT is a negative regulator of the antiviral response

EGOT is located in the genome antisense to intronic sequences of the ITPR1 gene, the inositol 1,4,5-trisphosphate receptor (Fig EV2). However, we did not observe a correlation between EGOT and ITPR1 expression, as HCV infection increases EGOT but it does not alter ITPR1 levels. To perform a stringent high-throughput analysis of correlation between the levels of EGOT and ITPR1, and to predict the function of EGOT with a high statistical confidence, we carried out a guilt-by-association genome-wide analysis [35]. To this end, we compared the expression levels of EGOT and coding genes related to cellular antiviral pathways, used as positive controls, with the expression levels of all the genes represented in a SurePrint G3 microarray. We used expression data from microarray experiments performed with 120 human samples of different origin (see Materials and Methods). Again, the results showed no significant correlation between EGOT and ITPR1 (correlation −0.23). The correlation analyses between each candidate and all the microarray genes were sorted from the genes with the highest positive correlation to those with the highest negative correlation. This matrix was used to search for GO categories with highly significant enrichment in genes that correlate positively (positive z-score) or negatively (negative z-score) with EGOT. This guilt-by-association genome-wide analysis revealed that EGOT has a highly significant negative correlation with genes that significantly enriched GO categories related to the innate immune response, including TLR signaling and the NF-κB pathway (Fig EV4). Therefore, EGOT clusters away from other genes related with the IFN pathway and the antiviral response, such as TLR3, NF-κB, IRF3, IFNAR2, or IRF1, which show a positive correlation with the antiviral pathway.

The results obtained thus far indicate that EGOT is required for efficient infection and correlates negatively with genes related to the innate immune response, suggesting that it could function by blocking antiviral responses. To test this hypothesis, we evaluated by qRT–PCR the levels of several ISGs in the HCV samples described in Fig 7, obtained from cells transfected with gapmers targeting EGOT or controls and infected with HCV for 48 h. Under these conditions, EGOT and HCV RNA levels were decreased (Fig 7A and B) while a significant increase was observed in the expression of several ISGs, including GBP1, ISG15, Mx1, BST2, ISG56, IFI6, and IFITM1 (Fig 8A and Appendix Fig S5A). No significant differences were observed in other ISGs such as IFITM2. Increased levels of ISGs were not observed when gapmers that target UCA1 were used as a control (Appendix Fig S5B). A similar increase in ISG expression was observed in non-infected cells treated with EGOT gapmers for 72 h (Fig 8B). Kinetics experiments were performed by transfecting the gapmers, infecting with HCV 24 h later and collecting the cells at 12 and 24 hpi. The results show that increased levels of GBP1 and ISG15 were observed in EGOT-depleted cells already at 12 hpi (Fig 8C and data not shown). However, at this time point there were no differences in HCV RNA levels between controls and silenced cells (Fig 8C). Decreased levels of HCV RNA were observed in EGOT-depleted cells at 24 hpi. This indicates that EGOT effect on ISGs precedes the effect on viral replication.

Discussion

Transcriptome analysis has allowed the identification of cellular lncRNAs induced in response to HCV infection (Fig 1 and Appendix Table S1). Out of the 35 CSRs selected, 33 were validated as upregulated after HCV infection. For further studies, we chose 10 candidates with medium-to-high expression levels that increased more than sevenfold after infection with HCV (Fig 2). We were surprised to find that several CSRs had been previously described in association with tumors. CAS15/CSR19 is a cancer susceptibility candidate with SNPs reported to be associated with clinically aggressive neuroblastoma [36]. UCA1/CSR34 and PVT1/CSR21 are well-described oncogenes upregulated in several tumors, including liver tumors, where upregulation is associated with poor prognosis [24,25,37]. It has been demonstrated that upregulation of UCA1 and PVT1 leads to increased cell proliferation. This allows us to hypothesize that the upregulation of several CSRs by HCV, including PVT-1, UCA1, and CASC15, could activate cell proliferation and several pro-carcinogenic processes that may contribute, in the long term, to the development of HCC in HCV-infected livers. Similarly, the X protein of HBV has been shown to decrease the expression of the lncRNA DREH, which functions as a tumor suppressor [38].

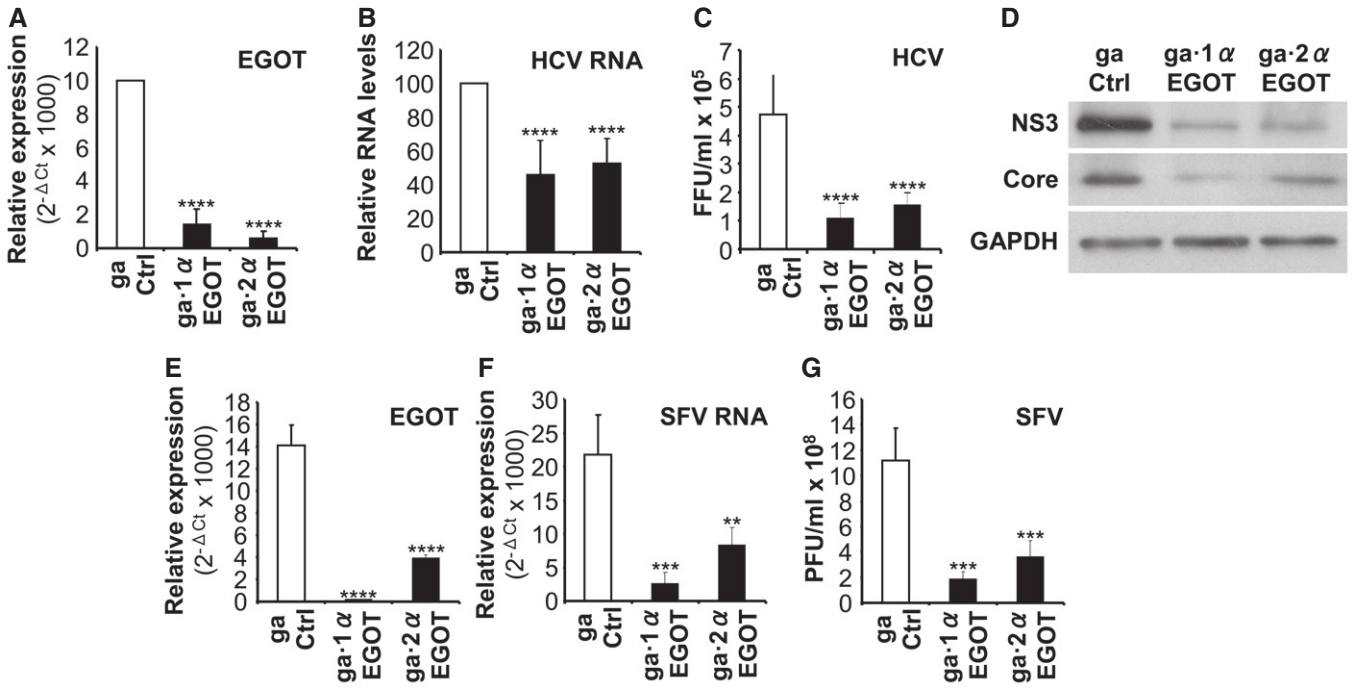

Figure 7. EGOT depletion interferes with viral replication.

A–G HuH7 cells were transfected with a control gapmer (ga Ctrl) or with two gapmers targeting EGOT (ga·1α EGOT and ga·2α EGOT). One day later, the cells were infected with a moi 0.3 of HCV for 48 h (A–D) or with a moi of 0.01 of SFV for 24 h (E and F). Cell supernatants and pellets were collected after infection. RNA was isolated from the cells to evaluate the levels of EGOT (A and E), HCV RNA (B), SFV RNA (F), and GAPDH mRNA, used as a reference to calculate the relative levels of the RNAs. Control HCV RNA has been set to 100% and represents values around 10^7 GE/μg of total RNA. NS3, core, and GAPDH proteins were evaluated by Western blot (D). The supernatant was used to titer the SFV by the plaque-forming assay (G) or the HCV virus by infecting fresh cells, counting core-expressing cells versus total cells, and calculating the focus-forming units per ml (FFU/ml) (C). The experiment was performed at least twice in triplicate (n = 6). Average values are shown, and error bars indicate standard deviations. Asterisks mark significant differences (**$P \leq 0.01$, ***$P \leq 0.001$, and ****$P \leq 0.0001$) obtained with a two-tailed t-test. PFU, plaque-forming units.

PVT1 expression increases the levels of myc protein, leading to increased proliferation [24]. Interestingly, PVT1 promoter responds to myc leading to a positive regulatory loop [24,39]. Myc is also increased by NS5A after infection with HCV [40]. Therefore, HCV infection could cause a myc upregulation that increases PVT1 levels, which, in turn, increase the myc protein. Upregulation of other CSRs could also be mediated by myc or by other viral or cellular factors related to HCV infection. In agreement with this possibility, CSR19, 21, 26, or 34 are not induced by IFN, pIC or by infection with influenza or SFV (Fig 3, Appendix Fig S3). In turn, other CSRs may be induced by transcription factors involved in the synthesis of IFN and the IFN response, which are activated in response to HCV infection [13] (Fig 1C). In fact, some CSRs are induced after transfection of pIC or treatment with IFN, although the level of induction obtained with these treatments is much lower than that with HCV infection (Fig 3). In addition, the promoters of several CSRs contain binding sites for myc or IFN-related transcription factors, as identified by ChIP-Seq analysis performed by ENCODE or evaluation of conserved transcription factor binding sites deposited at UCSC [41] (Appendix Table S3).

We studied EGOT/CSR32 in more detail. EGOT is a polyadenylated noncoding RNA found, at least, in all placental mammals that contains several evolutionary conserved and thermodynamically stable secondary structures [28] (Fig EV2). EGOT is expressed during eosinophil development and in mature eosinophils where it serves to regulate the expression of toxic eosinophil proteins, such as the major basic protein and the eosinophil-derived neurotoxin [42]. Although EGOT has been described to be a lncRNA preferentially expressed in the hematopoietic system, in this study we show that EGOT expression is increased in HuH7 cells (Figs 2–5) and in the liver of patients infected with HCV (Fig 6A). We believe that this could represent increased expression in hepatocytes rather than in immune cells infiltrated in the infected liver because (i) we do not observe a significant correlation between the levels of EGOT and the levels of CD68, CD56, CD4, and CD8B mRNA markers that were used to quantify macrophages, NK cells, CD4, and CD8 T lymphocytes, respectively, and (ii) EGOT levels were very low in human PBMCs and they did not increase when PBMCs obtained from healthy donors were incubated for 8 h with IFNα, LPS, or pIC (data not shown). Instead, EGOT increases markedly in HuH7 cells after infection with HCV and treatment with IFN, TLR agonists, or TNFα (Figs 2–5). Infection is detected by RIG-I and PKR, which activate NF-κB signaling and EGOT transcription (Fig 5). In agreement with this, EGOT is also upregulated after infection with other RNA viruses such as influenza virus or SFV (Fig 4A and B). Furthermore, in HuH7 cells we find a correlation between the levels of HCV RNA and the levels of EGOT (Fig 4). EGOT levels increased significantly at very early times post-infection or in cells infected with

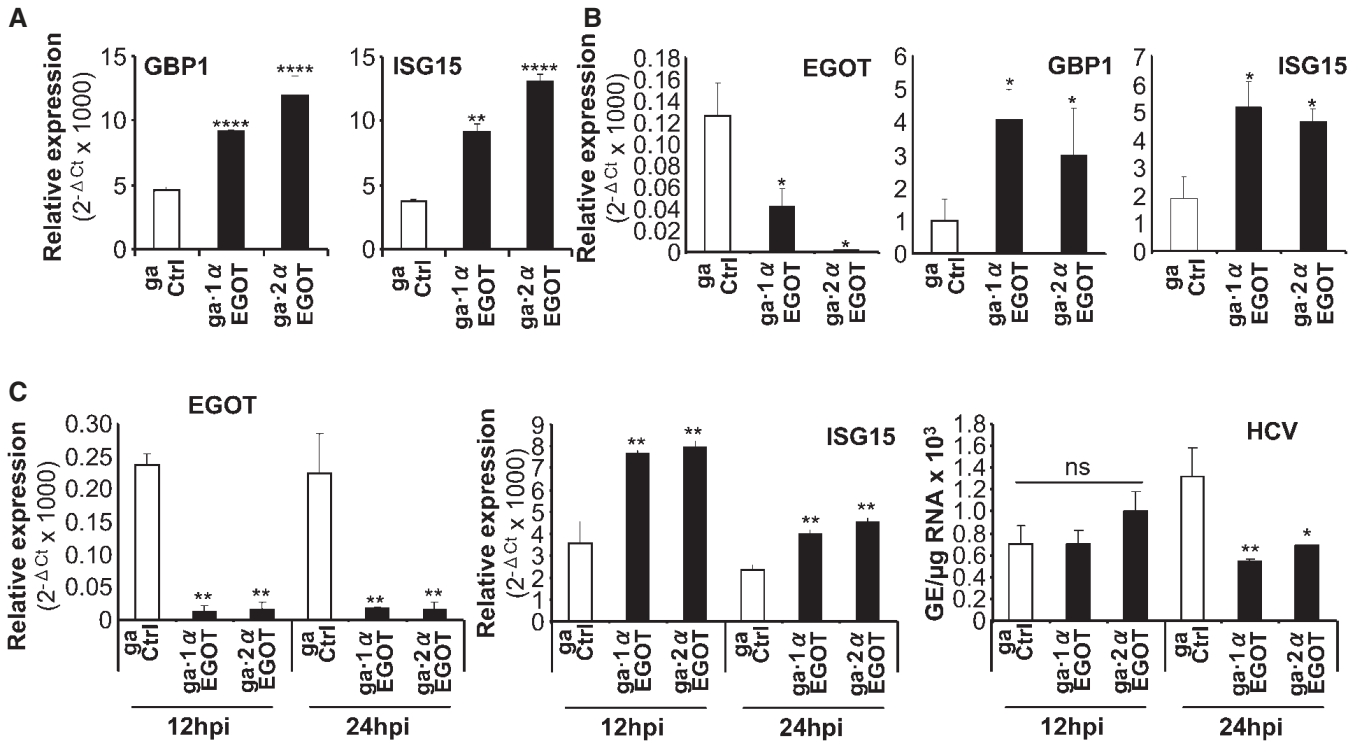

Figure 8. EGOT is a negative regulator of the antiviral response.

A The mRNA levels of the indicated ISGs were evaluated by qRT–PCR in RNA isolated from the HuH7 cells described in Fig 7A.

B HuH7 cells were transfected with a control gapmer or with two gapmers targeting EGOT and RNA was isolated 72 h post-transfection. Then, the levels of EGOT, ISG15, and GBP1 mRNAs were evaluated by qRT–PCR.

C HuH7 cells were transfected with a control gapmer or with two gapmers targeting EGOT. One day later, the cells were infected with a moi 0.3 of HCV for 12 and 24 h. RNA was isolated and the levels of EGOT and ISG15 mRNA and the genome equivalents of HCV (GE)/µg of total RNA were evaluated by qRT–PCR.

Data information: The experiments were performed at least twice in triplicate ($n = 6$). Average values are shown and error bars indicate standard deviations. Asterisks mark significant differences (ns, nonsignificant, *$P \leq 0.05$, **$P \leq 0.01$, ****$P < 0.001$) obtained with a two-tailed nonparametric Mann–Whitney *U*-test.

non-replicative UV-treated HCV viruses, suggesting that EGOT may increase in response to the detection of the incoming viral genome (Fig 4D). At later times post-infection, EGOT increases substantially while inhibition of viral replication causes a similar decrease in EGOT levels (Fig 4C).

Surprisingly, we did not observe a significant correlation between HCV RNA and EGOT in the liver of patients infected with HCV (Fig 6B). Of note, it has been reported that not all hepatocytes are infected with HCV in human livers. The proportion of HCV-infected hepatocytes per patient ranges from 21 to 45%, and most infected hepatocytes express low levels of viral RNA (between 1–7 to 8–64 molecules depending on the study [43–45]). Instead, we find a significant correlation between the levels of TNFα mRNA and EGOT, suggesting that this cytokine could be the major driver of EGOT expression in the liver of HCV-infected patients (Fig 6B). Given the complexity of the HCV cell cycle, we hypothesize that the levels of HCV RNA in patients could reflect the influence of several factors and EGOT could be one of these factors based on the experiments performed in HuH7 cells (Fig 7A–D). Finally, our results do not support an oncogenic role of EGOT in HCC. However, a larger cohort of well-characterized patients should be evaluated to address whether the levels of EGOT correlate with patient survival or response to treatment.

Guilt-by-association studies indicated that EGOT correlates negatively with genes related to the immune response, suggesting that it could be a negative regulator of the pathway (Fig EV4). In fact, inhibition of EGOT leads to increased levels of several ISGs (Fig 8). This is observed in both HCV-infected and in naïve cells, where EGOT expression is very low. In this case, we hypothesize that EGOT could be expressed in a subpopulation of cells where ISG control is important. Alternatively, if EGOT is not very stable, it could be expressed transiently in most cells with time. If this is the case, EGOT may have been inhibited in many cells during the three days of the inhibition experiment. Some of the ISGs affected by EGOT repression have already been described as blocking HCV or SFV entry, replication, or release [46–51]. Therefore, it is not surprising that once EGOT silencing has led to increased levels of ISGs, a decrease of HCV or SFV replication is observed (Figs 7 and 8). However, we cannot rule out the possibility that EGOT affects viral replication in an ISG-independent manner, for instance through regulation of ITPR. Further experiments are required to understand the molecular mechanisms that allow EGOT to affect expression of some antiviral genes. In fact, the repressive role of EGOT resembles what has been recently described for the lncRNAs NRIR and NRAV [3,10]. LncCMPK2/NRIR and NRAV are negative regulators of the IFN pathway induced by IFN or by infection. In fact,

downregulation of lncCMPK2/NRIR or NRAV lncRNA activates ISG transcription and inhibits HCV or influenza replication, respectively.

EGOT is the first lncRNA described to be induced by PKR (Fig 5). PKR is a well-studied antiviral factor activated by binding of viral dsRNA molecules or pIC analogues [29]. After activation, PKR inhibits translation initiation by phosphorylation of eIF2α. Many viruses, including SFV and HCV, have mechanisms that avoid the translation blockage exerted by PKR [30,52]. In fact, in the case of HCV, PKR is a proviral factor. Early after infection, HCV-activated PKR induces NF-κB and IRF3 and transcription of ISG15. ISG15 blocks the RIG-I pathway leading to decreased expression of several ISGs [29]. This favors HCV replication. Our study describes a novel pathway for PKR-mediated decrease of ISGs in HCV-infected cells. HCV-activated PKR induces NF-κB and transcription of EGOT, which decreases ISG expression (Figs 7 and 8). We hypothesize that this pathway may be relevant at later times post-HCV infection. At this time, translation initiation has been blocked by PKR activation and expression of lncRNAs, which do not require translation for functionality, may be essential to regulate the antiviral properties of the cell. Further studies will be required to elucidate the role of EGOT and other CSRs in viral infection. We believe that these studies will help to delineate the complex cellular response to infection with HCV and, probably, with other viruses and may lead to the discovery of new antivirals.

Materials and Methods

Cells, mice, and patient samples

The HuH7 and HuH7.5 cell lines, derived from a human hepatocarcinoma, were provided by Dr. Chisari's laboratory (Scripps Research Institute, La Jolla, CA, USA). BHK cells were provided by Dr. Liljeström's laboratory (Karolinska Institute, Stockholm, Sweden). Human liver samples with or without HCV infection were obtained from the Biobank of the University of Navarra (Pamplona, Spain) under approval from the Ethics and Scientific Committees. Liver tissue sections were snap-frozen and stored at −80°C. The clinical data from HCV-infected subjects are shown in Appendix Table S4. Animal studies were performed following the regulations of the Animal Care Ethics Committee from the University of Navarra. New born (12–15 days) C57BL/6 male mice (n = 23) were treated with 25 mg/kg of diethylnitrosamine (DEN, Sigma). Seven C57BL/6 mice were used as controls. Animals were sacrificed 9 months after DEN treatment. Healthy livers from untreated animals and peritumoral and tumoral tissue from DEN-treated animals were snap-frozen and stored at −80°C.

Cell culture, fractionations, and treatments

HuH7 and HuH7.5 cells were cultured in Dulbecco's modified Eagle's medium (DMEM; Invitrogen) enriched with 10% fetal bovine serum (FBS), 2 mM glutamine, 100 μg/ml streptomycin, and 100 IU/ml penicillin at 37°C in a 5% CO_2 atmosphere. The hamster cell line BHK-21 (ATCC-CCL10), used for SFV production and titration, was grown with Glasgow MEM (Gibco BRL, UK) supplemented with 5% FBS, 10% tryptose phosphate broth, 2 mM glutamine, 20 mM HEPES, 100 μg/ml streptomycin, and 100 IU/ml penicillin (BHK-21 complete medium). Cells were checked periodically for the presence of mycoplasma with the MycoAlert mycoplasma detection kit (Lonza). Cell fractionation into nucleus and cytoplasm was performed from cell pellets as described [5]. Blood was obtained from three healthy donors through the Biobank of the University of Navarra (Pamplona, Spain) under approval from the Ethics and Scientific Committees. Peripheral blood mononuclear cells (PBMCs) were selected after density gradient centrifugation using Ficoll.

PBMCs were cultured at a density of 10^6 cells/ml in RPMI media (Gibco) and mock-treated or treated with 2,500 U/ml of IFNα (Sicor Biotech, Lithuania), 5 μg/ml of lipopolysaccharide (LPS, DIFCO), and 15 μg/ml of poly I:C (pIC, Invivogen) for 6 h. HuH7 cells were seeded in 6-well plates 24 h before treatment. Then, they were transfected or treated with 10,000 units/ml of IFNα2 for 72 h (in all experiments except in Appendix Fig S3B, where the dose and time of IFNα are indicated in the figure legend), 20 ng/ml of TNFα for 6 or 12 h (PeproTech), 100 μg/ml of LPS for 24 h, 10 μg/ml of Imiquimod for 24 h (Invivogen), 10 μg/ml of oncostatin M (OSM) for 24 h (R&D System), or 10 ng/ml of IL-6 for 6 h (R&D System). Transfection was performed with 5 μl of Lipofectamine 2000 (Invitrogen) in 300 μl Optimem media (Gibco). For transfection, each 6-well plate received 10 μg of pIC, the indicated amounts of plasmids expressing PKR (cloned from pcDNAI/Neo-PKR [53] by E. Nistal (CIMA, Pamplona, Spain) in positions ClaI and XhoI of pCAGGS), 0.5 μg of pIKB(SA) [32], 0.5 μg of DN-IRF3 [31], a mixture of 0.5 μg of pNF-κB-Luc (NF-κB 3xLuc; Clontech), 0.25 μg of pRL-SV40 (expressing Renilla luciferase, Promega) and 0.5 μg of pIKB(SA) or pEGFP (Promega) or a mixture of 0.5 μg of pIRF3Luc (PRDIII-I)4-Luc; [33] 0.08 μg pIRF3 (expressing IRF3, [54]), 0.25 μg of pRL-SV40, and 0.5 μg of DN-IRF3 or pEGFP. For transfections with inhibitors, 40 pmol siRNAs targeting PKR or RIG-I or 50 pmol of gapmers targeting EGOT was transfected per 6-well plate. siRNAs target PKR at the sequence GCAGGGAGUAGUACUUAAA [55] and RIG-I at the sequence CGGAUUAGCGACAAAUUUA [56]. LNA™ longRNA GapmeR oligonucleotides (EXIQON) target the sequence AGAGACACTTAGAAGA (gaEGOT·1), GAGGTTAGGATGAAA (gaEGOT·2), or AACACGTCTATACGC (gaCtrl). UCA gapmer was obtained from IONIS Pharmaceuticals. One day post-transfection, media from the cells were substituted by fresh DMEM supplemented with 10% FBS and antibiotics.

Viral infections

HCV JFH-1 was obtained from an initial viral stock from the genotype 2a JFH-1 plasmid (pJFH-1), previously described by Wakita *et al* [57]. The virus was amplified as described [4]. For UV inactivation, the total amount of HCV to be used was exposed to a 254-nm UV light (three cycles of 15 min) by using an uvgl-25 compact UV 4-watt lamp (UVP). Cells were infected with HCV at a moi of 0.3 for 4 h. UV-treated virus was used with a moi of 1. After 4 h of infection, viruses were removed and fresh medium was added to the cells. Cell supernatants and pellets were harvested at the indicated times post-infection. Inhibition of replication was performed with a cocktail of 500 pM daclatasvir (Med Chem Express), 1,200 pM sofosbuvir (Med Chem Express), and 100 μM ribavirin (Sigma). To inhibit ongoing replication, cells were incubated with this cocktail 48 h after infection. To inhibit replication, cells were

treated with the cocktail 24 h before infection and immediately after infection. Then, the media with the inhibitors were replaced every 48 h until the end of the experiment.

To titer infectious HCV particles, we calculated focus-forming units/ml using a modified version of a previously described protocol [58]. In brief, the supernatant of infected cells was centrifuged at 1,700 *g* at 4°C for 15 min, serially diluted 10-fold in complete DMEM, and used to infect 10^5 naive HuH7 cells grown onto coverslips in 24-well plates. HCV infection was allowed to proceed for 2 days. Then, cells were fixed and permeabilized with methanol at −20°C for 15 min and used for immunofluorescence.

Influenza virus strain A/PR8/34 WT (PR8) was kindly provided by Estanislao Nistal (CIMA, Pamplona, Spain). A moi 10 of this virus was used to infect HuH7 cells for 1 h. RNA was isolated from infected cells at the indicated times post-infection. SFV was produced by electroporating BHK cells with SFV4 *in vitro*-transcribed RNA as described [59]. After 24 h, SFV viral particles were purified from the cultured supernatants by ultracentrifugation for 90 min at 100,000 g through a 20% sucrose cushion. The virus pellet was resuspended in TN buffer (50 mM Tris–HCl, pH 7.4, 100 mM NaCl), quickly frozen in liquid N_2, and stored at −80°C. HuH7 cells were infected with SFV for 1 h at a moi of 10 or 0.01, as indicated. To titer SFV, confluent BHK-21 cell monolayers were infected with serial dilutions of purified SFV, or cell supernatants containing SFV, diluted in infection medium (MEM containing 0.2% BSA, 2 mM glutamine, and 20 mM Hepes). After 1 h of viral adsorption, overlay medium was added (BHK-21 complete medium and Glasgow MEM-0.2% agarose, [1:1]) and cells were incubated for 72 h at 37°C. Finally, cell monolayers were fixed with 0.5% glutaraldehyde in PBS and stained with 0.1% crystal violet in methanol–H_2O (20:80), and viral lysis plaques were counted in the appropriate dilution.

Immunofluorescence, Western blot, and luciferase activity measurements

For immunofluorescence, cells fixed on coverslips were washed three times in PBS and incubated for 2 h at 37°C with a mouse monoclonal antibody against HCV core protein (a gift from J.J. Lasarte, CIMA, Pamplona, Spain) diluted 1:500. Then, the cells were washed three times with PBS and incubated for 2 h with a secondary anti-mouse antibody conjugated with Cγ3 diluted 1:200 (Sigma). Finally, the coverslips were washed and placed on a slide glass with VECTASHIELD Mounting Medium with DAPI (Vector Labs) [60]. Cells were visualized in a fluorescence microscope (Nikon Eclipse E800). Total cells stained with DAPI and core-positive cells stained with Cγ3 were quantified in the highest possible dilution with ImageJ (NIH). Fields continued to be evaluated until a stable average number of core-positive vs total cells was obtained. This value was used to calculate the focus-forming units per milliliter of supernatant [58].

For Western blot analysis, cell pellets were lysed in RIPA buffer and 20 μg of protein extracts was run through a 12% acrylamide gel and transferred onto a nitrocellulose membrane (Protran Whatman) [34]. After transfer, membranes were blocked with 5% milk in TBST for 1 h and incubated with monoclonal antibodies against GAPDH diluted 1:10,000 (Sigma), HCV NS3 protein diluted 1:1,000 (anti-NS3 (JFH-1) Monoclonal Clone 2E3 Biofront), HCV core protein diluted 1:1,000 or anti-phospho-PKR diluted 1:1,000 (phospho T446 antibody E120, Abcam). After washing, membranes were incubated with a secondary anti-mouse antibody conjugated with peroxidase diluted 1:5,000 (Sigma) except for recognition of phospho-PKR, where a secondary anti-rabbit antibody conjugated with peroxidase diluted 1:10,000 (Cell Signaling) was used. Western blots were developed with ECL Plus (PerkinElmer).

Renilla and firefly luciferase activities were measured using the Dual Luciferase System (Promega) as previously described [34] in a Berthold Luminometer (Lumat LB 9507). The values obtained for firefly luciferase were corrected for equal transfection efficiency with Renilla luciferase activity.

RNA extraction, RT–PCRs, and cloning

Human and mouse tissue was homogenized using the ULTRA-TURRAX dispersing machine (t25 basic IKA-WERKE) [61], and RNA was isolated as described [62]. DNase (Fermentas) treatment was performed to eliminate DNA from the samples. RNA from cell pellets was extracted with the MaxWell 16 research system from Promega following the manufacturer's recommendations. RNA concentration was measured using NanoDrop 1000 Spectrophotometer. The quality of the RNA was analyzed by Bioanalyzer (Agilent Technologies). Reverse transcription (RT) was performed as described [62]. An oligodT primer (T_{40}) was used in the RT reaction to determine whether EGOT is polyadenylated. Those candidates located in regions with transcription in the sense and antisense orientation were also evaluated with strand-specific PCR.

The quantitative RT–PCR (qRT–PCR) was performed in the C1000 Touch Thermal Cycler from Bio-Rad. The samples were incubated at 37°C for 60 min, then at 95°C for 60 s and then immediately cooled to 4°C. qPCR was performed in the CFX96 Real-Time System from Bio-Rad as described [63]. The results were analyzed with Bio-Rad CFX Manager software. GAPDH levels were evaluated in all the cases as a reference. Only samples with similar GAPDH amplification were analyzed further. To calculate the relative RNA levels, $2^{-\Delta Ct}$ was used, where $\Delta Ct = Ct$ of the gene of interest − Ct of the GAPDH mRNA internal control. The primers used are listed in Appendix Table S5 and were designed with the Primer3 program (http://frodo.wi.mit.edu).

EGOT RACE was performed with the 5′ and 3′RACE systems for rapid amplification of cDNA ends (Thermo Fisher) using the conditions recommended by the supplier and RNA extracted from HuH7 cells infected with HCV for 48 h. Amplified products were resolved in agarose gels and evaluated by sequencing. Similar PCR conditions were used to amplify EGOT with Thermo Scientific Phusion High-Fidelity DNA Polymerase (Thermo Fisher). Primers used were cEGOT forward and reverse (Appendix Table S5). The amplified product was digested with XhoI and BglII and cloned into the same sites of pCAGGS to obtain pCAGGS-EGOT. Positive clones were verified by sequencing to confirm that the exon junction and EGOT sequence are identical to what has been annotated in several public databases (ENCODE, RefSeq, and ENSEMBL). pCAGGS-EGOT was then digested with SmaI and BglII and cloned into the same sites of pSuper to obtain pSuper-EGOT, which positions EGOT under a T7 promoter.

pSuper-EGOT was digested with ClaI and used in an *in vitro* transcription reaction with T7 (Promega) as described previously

[64]. Then, DNA was digested with RNase-free DNase (Promega) and RNA was quantified by bioanalyzer. Five nanograms of RNA was retrotranscribed as described, and serial dilutions 1:10 were used as a standard for a qPCR. The levels of EGOT in HCV-infected HuH7 cells and controls were evaluated in parallel, and absolute quantification was performed. Similarly, the levels of HCV RNA were determined in parallel with serial dilutions of a plasmid containing the HCV JFH-1 cDNA, which were used as a standard in the qPCR and allowed the calculation of HCV RNA genome equivalents (GE)/μg of total RNA as has been previously described [58].

Microarray hybridization and high-throughput sequencing

RNA of excellent quality, as determined by Bioanalyzer (Agilent Technologies), was hybridized to microarrays or used for high-throughput sequencing. For microarray hybridization, the samples were processed using manufacturer protocols and hybridized to the Agilent SurePrint G3 Human Gene Expression 8x60K microarray. Microarray data normalization was performed using the quantile algorithm and analyzed as described [65]. For RNASeq, RNA was treated with the Ribo-Zero rRNA removal kit (Epicenter) to deplete ribosomal RNA. Library preparation with the TruSeq RNA sample preparation kit (Illumina) and sequencing was performed at the EMBL genomics core facility (Genecore) in an Illumina HiSeq 2000. Sequences were paired-end, 105 bases long, and strand specific. RNASeq data analysis was performed as described [5]. Further analysis and graphical representations were performed using an R/Bioconductor [66]. The biological knowledge extraction was complemented through the use of Ingenuity Pathway Analysis (Ingenuity Systems, www.ingenuity.com). All transcriptome data are available at the NCBI Gene Expression Omnibus (GEO) data repository (http://www.ncbi.nlm.nih.gov/geo).

Bioinformatic analysis

Reads from all the differentially expressed genomic regions were visualized in the Integrative Genomics Viewer (IGV) (www.broadinstitute.org/igv), the sequences were compared to the ENSEMBL and ENCODE databases, and more information was searched for in the Genome Browser from UCSC (http://genome.ucsc.edu) [67,68] Candidates were divided into coding, noncoding (according to UCSC classification), or non-assigned, when the transcription of the sequence had not been annotated in the databases. ORF Finder (NCBI) was used to evaluate the length of all probable ORFs in the evaluated transcripts. Coding potential was assayed with Phylogenetic Codon Substitution Frequencies (PhyloCSF) [20,23], the coding potential assessment tool (CPAT) [22], and by searching the LNCipedia database [20]. PhyloCSF uses multiple alignments to calculate the phylogenetic conservation score and determines whether a multispecies nucleotide sequence alignment is likely to represent a protein-coding region [23]. CPAT uses a model built with open reading frame size and coverage together with codon (Ficket score) and hexamer (hexamer score) usage bias to calculate a coding probability value. Human noncoding transcripts have a coding probability value lower than 0.364, used as a threshold with the highest sensitivity and specificity [22]. The LNCipedia database evaluates the presence of transcripts in the PRIDE Archive, a database for proteomic data, or in the Lee or Bazzini lists of transcripts associated with ribosomes in ribosome profiling experiments [18,19,21].

The Illumina Human BodyMap (HBM) dataset was downloaded from SRA database and processed using the following pipeline: (i) The preprocessing of reads included elimination of contaminating adapter substrings was performed with Scythe (https://github.com/vsbuffalo/scythe) and the quality-based trimming was done using Sickle (https://github.com/najoshi/sickle); (ii) the alignment of reads to the human genome (hg19) was performed using Tophat2 mapper; and (iii) the quantification of the 37 CSRs using the FPKM (fragments per kilobase of transcript per million fragments mapped) was carried out with Cuffquant.

To perform the guilt-by-association analysis [35], we collected data from 120 samples hybridized to SurePrint G3 microarrays. These samples included the 6 RNA samples isolated from HuH7 cells infected or not with HCV, and 114 RNAs obtained from human samples of different origin, including healthy cells and tissues (one sample from CD34 cells, 3 from fibroblasts, 15 colon samples, 8 rectum samples, and 3 peripheral blood samples), tumors (20 colon cancers (GSE46271), 8 rectal cancers, 9 colon metastases, 3 acute lymphoblastic leukemias from B cells and one from T cells), cell lines (7 MOLT4, 1 Tera, 10 TOM1, one DLD1, one LS513, one HT29, one SW620), cell line-derived cancer stem cells (one derived from DLD1, one from LS513, one from HT29, and one from SW620), stem cells (3 adipose-derived stem cells, 6 IPS cells derived from fibroblasts, and 2 derived from CD34 cells), and 6 samples of HuH7 cells treated with IFN (GSE64794). Then, a Pearson correlation analysis was performed between CSR32 and all the genes represented in the SurePrint G3 Human microarray. Coding genes related to cellular antiviral pathways were randomly selected and included in the analysis as positive controls. The obtained correlation matrix was used as input for giTools [69] where an enrichment analysis of GO categories was performed using z-score and FDR [70].

Statistical analysis

Statistical analysis was performed using GraphPad. Statistical significance of treated or infected versus non-treated or non-infected samples was calculated using a two-tailed nonparametric Mann–Whitney *U*-test for samples that do not follow a normal distribution. When the samples followed a normal distribution according to the Shapiro–Wilk test, a two-tailed Student's *t*-test was used. Correlation was assessed by Spearman's correlation coefficients. All data show means ± standard deviation. *P*-values lower than 0.05 were deemed as significant. In all data shown, * denotes $P \leq 0.05$, ** $P \leq 0.01$, *** $P \leq 0.001$, and **** $P \leq 0.0001$.

Expanded View for this article is available online.

Acknowledgements

We thank Nerea Razquin and Erkuden Casales for excellent technical assistance, Paul Miller for editorial work, and Estanislao Nistal and Rafael Aldabe for influenza and HCV, respectively. We also thank Estanislao Nistal for the plasmid expressing PKR, DN-IRF3, IRF3, and IκB(SA), Esther Larrea for IFNα2, LPS, IL-6, and oncostatin, Stephan Ludwig for (PRDIII-I)4-Luc, Pablo Sarobe for Imiquimod, Juanjo Lasarte for the antibody against HCV core protein, Lulu Huang, from IONIS Pharmaceuticals, for UCA1 gapmers, Sandra Herbás for

PBMCs, Celia Perales for help with the HCV replication inhibitors, and Marta Ruiz-Guillen for providing purified SFV. We would like to thank patients for the generous donation of samples and Virginia Villar and the biobank of the University of Navarra for their mediation. This work was supported by grants from the Ministry of Economy (SAF2012-40003, BFU2013-50517-EXP, SAF2015-70971-R), grant Ortiz de Landazuri from the Government of Navarra, Fundacio La Marato de TV3 (20132130-31-32), Caja Navarra Foundation (70020), European FEDER funding and by the project RNAREG [CSD2009-00080], funded by the Ministry of Science and Innovation under the program CONSOLIDER INGENIO 2010. MB is the recipient of a FPI fellowship.

Author contributions

EC performed initial analysis and validation of CSRs and together with MB and CP, the analysis of EGOT functionality; VS was in charge of all the bioinformatics analysis except the guilt-by-association studies that were carried out by EG; CS performed all experiments related to SFV and PG experiments with replication inhibitors; JPU was in charge of the RACE experiments, ME obtained and analyzed mouse samples, and PF conceived the project and the required experiments, provided the budget, led the team in the analysis and interpretation of the data, and wrote the manuscript.

Conflict of interest

The authors declare that they have no conflict of interest.

References

1. Schneider WM, Chevillotte MD, Rice CM (2014) Interferon-stimulated genes: a complex web of host defenses. *Annu Rev Immunol* 32: 513 – 545
2. Oliere S, Hernandez E, Lezin A, Arguello M, Douville R, Nguyen TL, Olindo S, Panelatti G, Kazanji M, Wilkinson P *et al* (2010) HTLV-1 evades type I interferon antiviral signaling by inducing the suppressor of cytokine signaling 1 (SOCS1). *PLoS Pathog* 6: e1001177
3. Kambara H, Niazi F, Kostadinova L, Moonka DK, Siegel CT, Post AB, Carnero E, Barriocanal M, Fortes P, Anthony DD *et al* (2014) Negative regulation of the interferon response by an interferon-induced long non-coding RNA. *Nucleic Acids Res* 42: 10668 – 10680
4. Carnero E, Barriocanal M, Segura V, Guruceaga E, Prior C, Borner K, Grimm D, Fortes P (2014) Type I interferon regulates the expression of long non-coding RNAs. *Front Immunol* 5: 548
5. Barriocanal M, Carnero E, Segura V, Fortes P (2015) Long non-coding RNA BST2/BISPR is induced by IFN and regulates the expression of the antiviral factor Tetherin. *Front Immunol* 5: 655
6. Kambara H, Gunawardane L, Zebrowski E, Kostadinova L, Jobava R, Hatzoglou M, Anthony DD, Valadkhan S (2015) Regulation of Interferon-stimulated gene BST2 by a lncRNA transcribed from a shared bidirectional promoter. *Front Immunol* 5: 676
7. Fatica A, Bozzoni I (2014) Long non-coding RNAs: new players in cell differentiation and development. *Nat Rev Genet* 15: 7 – 21
8. Winterling C, Koch M, Koeppel M, Garcia-Alcalde F, Karlas A, Meyer TF (2014) Evidence for a crucial role of a host non-coding RNA in influenza A virus replication. *RNA Biol* 11: 66 – 75
9. Zhang Q, Chen CY, Yedavalli VS, Jeang KT (2013) NEAT1 long noncoding RNA and paraspeckle bodies modulate HIV-1 posttranscriptional expression. *MBio* 4: e00596-12
10. Ouyang J, Zhu X, Chen Y, Wei H, Chen Q, Chi X, Qi B, Zhang L, Zhao Y, Gao GF *et al* (2014) NRAV, a long noncoding RNA, modulates antiviral responses through suppression of interferon-stimulated gene transcription. *Cell Host Microbe* 16: 616 – 626
11. Fortes P, Morris KV (2016) Long noncoding RNAs in viral infections. *Virus Res* 212: 1 – 11
12. Carnero E, Fortes P (2016) HCV infection, IFN response and the coding and non-coding host cell genome. *Virus Res* 212: 85 – 102
13. Blackham S, Baillie A, Al-Hababi F, Remlinger K, You S, Hamatake R, McGarvey MJ (2010) Gene expression profiling indicates the roles of host oxidative stress, apoptosis, lipid metabolism, and intracellular transport genes in the replication of hepatitis C virus. *J Virol* 84: 5404 – 5414
14. Li Q, Pene V, Krishnamurthy S, Cha H, Liang TJ (2013) Hepatitis C virus infection activates an innate pathway involving IKK-alpha in lipogenesis and viral assembly. *Nat Med* 19: 722 – 729
15. Colman H, Le Berre-Scoul C, Hernandez C, Pierredon S, Bihouee A, Houlgatte R, Vagner S, Rosenberg AR, Feray C (2013) Genome-wide analysis of host mRNA translation during hepatitis C virus infection. *J Virol* 87: 6668 – 6677
16. Marin-Bejar O, Marchese FP, Athie A, Sanchez Y, Gonzalez J, Segura V, Huang L, Moreno I, Navarro A, Monzo M *et al* (2013) Pint lincRNA connects the p53 pathway with epigenetic silencing by the Polycomb repressive complex 2. *Genome Biol* 14: R104
17. Kretz M, Siprashvili Z, Chu C, Webster DE, Zehnder A, Qu K, Lee CS, Flockhart RJ, Groff AF, Chow J *et al* (2013) Control of somatic tissue differentiation by the long non-coding RNA TINCR. *Nature* 493: 231 – 235
18. Bazzini AA, Johnstone TG, Christiano R, Mackowiak SD, Obermayer B, Fleming ES, Vejnar CE, Lee MT, Rajewsky N, Walther TC *et al* (2014) Identification of small ORFs in vertebrates using ribosome footprinting and evolutionary conservation. *EMBO J* 33: 981 – 993
19. Lee S, Liu B, Lee S, Huang SX, Shen B, Qian SB (2012) Global mapping of translation initiation sites in mammalian cells at single-nucleotide resolution. *Proc Natl Acad Sci USA* 109: E2424 – E2432
20. Volders PJ, Helsens K, Wang X, Menten B, Martens L, Gevaert K, Vandesompele J, Mestdagh P (2013) LNCipedia: a database for annotated human lncRNA transcript sequences and structures. *Nucleic Acids Res* 41: D246 – D251
21. Vizcaino JA, Cote RG, Csordas A, Dianes JA, Fabregat A, Foster JM, Griss J, Alpi E, Birim M, Contell J *et al* (2013) The PRoteomics IDEntifications (PRIDE) database and associated tools: status in 2013. *Nucleic Acids Res* 41: D1063 – D1069
22. Wang L, Park HJ, Dasari S, Wang S, Kocher JP, Li W (2013) CPAT: Coding-Potential Assessment Tool using an alignment-free logistic regression model. *Nucleic Acids Res* 41: e74
23. Lin MF, Jungreis I, Kellis M (2011) PhyloCSF: a comparative genomics method to distinguish protein coding and non-coding regions. *Bioinformatics* 27: i275 – i282
24. Tseng YY, Moriarity BS, Gong W, Akiyama R, Tiwari A, Kawakami H, Ronning P, Reuland B, Guenther K, Beadnell TC *et al* (2014) PVT1 dependence in cancer with MYC copy-number increase. *Nature* 512: 82 – 86
25. Huang J, Zhou N, Watabe K, Lu Z, Wu F, Xu M, Mo YY (2014) Long non-coding RNA UCA1 promotes breast tumor growth by suppression of p27 (Kip1). *Cell Death Dis* 5: e1008
26. Takeuchi O, Akira S (2008) MDA5/RIG-I and virus recognition. *Curr Opin Immunol* 20: 17 – 22
27. Heintzman ND, Stuart RK, Hon G, Fu Y, Ching CW, Hawkins RD, Barrera LO, Van Calcar S, Qu C, Ching KA *et al* (2007) Distinct and predictive chromatin signatures of transcriptional promoters and enhancers in the human genome. *Nat Genet* 39: 311 – 318

28. Rose D, Stadler PF (2011) Molecular evolution of the non-coding eosinophil granule ontogeny transcript. *Front Genet* 2: 69
29. Arnaud N, Dabo S, Akazawa D, Fukasawa M, Shinkai-Ouchi F, Hugon J, Wakita T, Meurs EF (2011) Hepatitis C virus reveals a novel early control in acute immune response. *PLoS Pathog* 7: e1002289
30. Garaigorta U, Chisari FV (2009) Hepatitis C virus blocks interferon effector function by inducing protein kinase R phosphorylation. *Cell Host Microbe* 6: 513 – 522
31. Martinez-Sobrido L, Zuniga EI, Rosario D, Garcia-Sastre A, de la Torre JC (2006) Inhibition of the type I interferon response by the nucleoprotein of the prototypic arenavirus lymphocytic choriomeningitis virus. *J Virol* 80: 9192 – 9199
32. Wang X, Li M, Zheng H, Muster T, Palese P, Beg AA, Garcia-Sastre A (2000) Influenza A virus NS1 protein prevents activation of NF-kappaB and induction of alpha/beta interferon. *J Virol* 74: 11566 – 11573
33. Ehrhardt C, Kardinal C, Wurzer WJ, Wolff T, von Eichel-Streiber C, Pleschka S, Planz O, Ludwig S (2004) Rac1 and PAK1 are upstream of IKK-epsilon and TBK-1 in the viral activation of interferon regulatory factor-3. *FEBS Lett* 567: 230 – 238
34. Abad X, Razquin N, Abad A, Fortes P (2010) Combination of RNA interference and U1 inhibition leads to increased inhibition of gene expression. *Nucleic Acids Res* 38: e136
35. Ashburner M, Ball CA, Blake JA, Botstein D, Butler H, Cherry JM, Davis AP, Dolinski K, Dwight SS, Eppig JT *et al* (2000) Gene ontology: tool for the unification of biology. The Gene Ontology Consortium. *Nat Genet* 25: 25 – 29
36. Maris JM, Mosse YP, Bradfield JP, Hou C, Monni S, Scott RH, Asgharzadeh S, Attiyeh EF, Diskin SJ, Laudenslager M *et al* (2008) Chromosome 6p22 locus associated with clinically aggressive neuroblastoma. *N Engl J Med* 358: 2585 – 2593
37. Srivastava AK, Singh PK, Rath SK, Dalela D, Goel MM, Bhatt ML (2014) Appraisal of diagnostic ability of UCA1 as a biomarker of carcinoma of the urinary bladder. *Tumour Biol* 35: 11435 – 11442
38. Huang JF, Guo YJ, Zhao CX, Yuan SX, Wang Y, Tang GN, Zhou WP, Sun SH (2013) Hepatitis B virus X protein (HBx)-related long noncoding RNA (lncRNA) down-regulated expression by HBx (Dreh) inhibits hepatocellular carcinoma metastasis by targeting the intermediate filament protein vimentin. *Hepatology* 57: 1882 – 1892
39. Carramusa L, Contino F, Ferro A, Minafra L, Perconti G, Giallongo A, Feo S (2007) The PVT-1 oncogene is a Myc protein target that is overexpressed in transformed cells. *J Cell Physiol* 213: 511 – 518
40. Higgs MR, Lerat H, Pawlotsky JM (2013) Hepatitis C virus-induced activation of beta-catenin promotes c-Myc expression and a cascade of pro-carcinogenetic events. *Oncogene* 32: 4683 – 4693
41. Lin JM, Collins PJ, Trinklein ND, Fu Y, Xi H, Myers RM, Weng Z (2007) Transcription factor binding and modified histones in human bidirectional promoters. *Genome Res* 17: 818 – 827
42. Wagner LA, Christensen CJ, Dunn DM, Spangrude GJ, Georgelas A, Kelley L, Esplin MS, Weiss RB, Gleich GJ (2007) EGO, a novel, noncoding RNA gene, regulates eosinophil granule protein transcript expression. *Blood* 109: 5191 – 5198
43. Chang M, Williams O, Mittler J, Quintanilla A, Carithers RL Jr, Perkins J, Corey L, Gretch DR (2003) Dynamics of hepatitis C virus replication in human liver. *Am J Pathol* 163: 433 – 444
44. Kandathil AJ, Graw F, Quinn J, Hwang HS, Torbenson M, Perelson AS, Ray SC, Thomas DL, Ribeiro RM, Balagopal A (2013) Use of laser capture microdissection to map hepatitis C virus-positive hepatocytes in human liver. *Gastroenterology* 145: 1404 – 1413. e1-10
45. Stiffler JD, Nguyen M, Sohn JA, Liu C, Kaplan D, Seeger C (2009) Focal distribution of hepatitis C virus RNA in infected livers. *PLoS ONE* 4: e6661
46. Itsui Y, Sakamoto N, Kakinuma S, Nakagawa M, Sekine-Osajima Y, Tasaka-Fujita M, Nishimura-Sakurai Y, Suda G, Karakama Y, Mishima K *et al* (2009) Antiviral effects of the interferon-induced protein guanylate binding protein 1 and its interaction with the hepatitis C virus NS5B protein. *Hepatology* 50: 1727 – 1737
47. Amet T, Byrd D, Hu N, Sun Q, Li F, Zhao Y, Hu S, Grantham A, Yu Q (2014) BST-2 expression in human hepatocytes is inducible by all three types of interferons and restricts production of hepatitis C virus. *Curr Mol Med* 14: 349 – 360
48. Raychoudhuri A, Shrivastava S, Steele R, Kim H, Ray R, Ray RB (2011) ISG56 and IFITM1 proteins inhibit hepatitis C virus replication. *J Virol* 85: 12881 – 12889
49. Wilkins C, Woodward J, Lau DT, Barnes A, Joyce M, McFarlane N, McKeating JA, Tyrrell DL, Gale M Jr (2013) IFITM1 is a tight junction protein that inhibits hepatitis C virus entry. *Hepatology* 57: 461 – 469
50. Landis H, Simon-Jodicke A, Kloti A, Di Paolo C, Schnorr JJ, Schneider-Schaulies S, Hefti HP, Pavlovic J (1998) Human MxA protein confers resistance to Semliki Forest virus and inhibits the amplification of a Semliki Forest virus-based replicon in the absence of viral structural proteins. *J Virol* 72: 1516 – 1522
51. Ooi YS, Dube M, Kielian M (2015) BST2/tetherin inhibition of alphavirus exit. *Viruses* 7: 2147 – 2167
52. Ventoso I, Sanz MA, Molina S, Berlanga JJ, Carrasco L, Esteban M (2006) Translational resistance of late alphavirus mRNA to eIF2alpha phosphorylation: a strategy to overcome the antiviral effect of protein kinase PKR. *Genes Dev* 20: 87 – 100
53. Tan SL, Gale MJ Jr, Katze MG (1998) Double-stranded RNA-independent dimerization of interferon-induced protein kinase PKR and inhibition of dimerization by the cellular P58IPK inhibitor. *Mol Cell Biol* 18: 2431 – 2443
54. Escalante CR, Nistal-Villan E, Shen L, Garcia-Sastre A, Aggarwal AK (2007) Structure of IRF-3 bound to the PRDIII-I regulatory element of the human interferon-beta enhancer. *Mol Cell* 26: 703 – 716
55. McAllister CS, Samuel CE (2009) The RNA-activated protein kinase enhances the induction of interferon-beta and apoptosis mediated by cytoplasmic RNA sensors. *J Biol Chem* 284: 1644 – 1651
56. Yoo JS, Takahasi K, Ng CS, Ouda R, Onomoto K, Yoneyama M, Lai JC, Lattmann S, Nagamine Y, Matsui T *et al* (2014) DHX36 enhances RIG-I signaling by facilitating PKR-mediated antiviral stress granule formation. *PLoS Pathog* 10: e1004012
57. Wakita T, Pietschmann T, Kato T, Date T, Miyamoto M, Zhao Z, Murthy K, Habermann A, Krausslich HG, Mizokami M *et al* (2005) Production of infectious hepatitis C virus in tissue culture from a cloned viral genome. *Nat Med* 11: 791 – 796
58. Zhong J, Gastaminza P, Cheng G, Kapadia S, Kato T, Burton DR, Wieland SF, Uprichard SL, Wakita T, Chisari FV (2005) Robust hepatitis C virus infection in vitro. *Proc Natl Acad Sci USA* 102: 9294 – 9299
59. Liljestrom P, Lusa S, Huylebroeck D, Garoff H (1991) In vitro mutagenesis of a full-length cDNA clone of Semliki Forest virus: the small 6,000-molecular-weight membrane protein modulates virus release. *J Virol* 65: 4107 – 4113
60. Fortes P, Lamond AI, Ortin J (1995) Influenza virus NS1 protein alters the subnuclear localization of cellular splicing components. *J Gen Virol* 76(Pt 4): 1001 – 1007

61. Narvaiza I, Aparicio O, Vera M, Razquin N, Bortolanza S, Prieto J, Fortes P (2006) Effect of adenovirus-mediated RNA interference on endogenous microRNAs in a mouse model of multidrug resistance protein 2 gene silencing. *J Virol* 80: 12236 – 12247
62. Blazquez L, Gonzalez-Rojas SJ, Abad A, Razquin N, Abad X, Fortes P (2012) Increased in vivo inhibition of gene expression by combining RNA interference and U1 inhibition. *Nucleic Acids Res* 40: e8
63. Sobrevals L, Enguita M, Rodriguez C, Gonzalez-Rojas J, Alzaguren P, Razquin N, Prieto J, Fortes P (2012) AAV vectors transduce hepatocytes in vivo as efficiently in cirrhotic as in healthy rat livers. *Gene Ther* 19: 411 – 417
64. Fortes P, Longman D, McCracken S, Ip JY, Poot R, Mattaj IW, Caceres JF, Blencowe BJ (2007) Identification and characterization of RED120: a conserved PWI domain protein with links to splicing and 3′-end formation. *FEBS Lett* 581: 3087 – 3097
65. Aparicio O, Carnero E, Abad X, Razquin N, Guruceaga E, Segura V, Fortes P (2010) Adenovirus VA RNA-derived miRNAs target cellular genes involved in cell growth, gene expression and DNA repair. *Nucleic Acids Res* 38: 750 – 763
66. Gentleman R, Carey V, Huber W, Irizarry R, Dudoit S (2005) *Bioinformatics and Computational Biology Solutions using R and Bioconductor*. New York, NY: Springer
67. Karolchik D, Barber GP, Casper J, Clawson H, Cline MS, Diekhans M, Dreszer TR, Fujita PA, Guruvadoo L, Haeussler M *et al* (2014) The UCSC Genome Browser database: 2014 update. *Nucleic Acids Res* 42: D764 – D770
68. Harrow J, Frankish A, Gonzalez JM, Tapanari E, Diekhans M, Kokocinski F, Aken BL, Barrell D, Zadissa A, Searle S *et al* (2012) GENCODE: the reference human genome annotation for The ENCODE Project. *Genome Res* 22: 1760 – 1774
69. Perez-Llamas C, Lopez-Bigas N (2011) Gitools: analysis and visualisation of genomic data using interactive heat-maps. *PLoS ONE* 6: e19541
70. Benjamini Y, Hochberg Y (1995) Controlling the false discovery rate: a practical and powerful approach to multiple testing. *J R Statist Soc B (Methodological)* 57: 289 – 300

